AGU PUBLICATIONS

JGR

Journal of Geophysical Research: Solid Earth

RESEARCH ARTICLE
10.1002/2016JB013025

Key Points:
- We apply digital image correlation to repeated sidescan sonar surveys to measure seafloor displacement
- This measurement is most accurate in the across-track (range) dimension
- This experiment requires a dual-frequency GPS receiver for positioning the ship

Correspondence to:
J. DeSanto,
jdesanto@ucsd.edu

Citation:
DeSanto, J. B., D. T. Sandwell, and C. D. Chadwell (2016), Seafloor geodesy from repeated sidescan sonar surveys, *J. Geophys. Res. Solid Earth*, *121*, 4800–4813, doi:10.1002/2016JB013025.

Received 28 MAR 2016
Accepted 12 JUN 2016
Accepted article online 17 JUN 2016
Published online 2 JUL 2016

Seafloor geodesy from repeated sidescan sonar surveys

John B. DeSanto[1], David T. Sandwell[1], and C. David Chadwell[1]

[1]Scripps Institution of Oceanography, University of California, San Diego, La Jolla, California, USA

Abstract Accurate seafloor geodetic methods are critical to the study of marine natural hazards such as megathrust earthquakes, landslides, and volcanoes. We propose digital image correlation of repeated shipboard sidescan sonar surveys as a measurement of seafloor deformation. We test this method using multibeam surveys collected in two locales: 2500 m deep lightly sedimented seafloor on the flank of a spreading ridge and 4300 m deep heavily sedimented seafloor far from any plate boundary. Correlation of these surveys are able to recover synthetic displacements in the across-track (range) direction accurate to within 1 m and in the along-track (azimuth) direction accurate to within 1–10 m. We attribute these accuracies to the inherent resolution of sidescan data being better in the range dimension than the azimuth dimension. These measurements are primarily limited by the accuracy of the ship navigation. Dual-frequency GPS units are accurate to ~10 cm, but single-frequency GPS units drift on the order of 1 m/h and are insufficient for geodetic application.

1. Introduction

1.1. Summary

There is a compelling need for accurate and economical tools to be used for seafloor geodetic applications [*Davis et al.*, 2012; *Wilcock et al.*, 2012]. The vast majority of plate margins, specifically the subduction zones associated with megathrust earthquake and tsunami hazards, are distributed in marine environments unobservable via traditional satellite-based techniques [*Spiess*, 1985]. Understanding the earthquake cycle along spreading ridges, transform faults, and subduction zones will require at least two types of geodetic measurements—point measurements to establish plate motions and spatially dense coverage to investigate moment accumulation rate of locked patches at the plate margins.

On land, these tools are well developed. Point measurements from GPS networks provide millimeter-accuracy, vector displacement time series [*Wdowinski et al.*, 2001], and interferometric synthetic aperture radar (InSAR) provides spatially dense snapshots of line-of-sight deformation [*Bürgmann et al.*, 2000]. However, these techniques make use of electromagnetic radiation which cannot penetrate the deep ocean.

There are three main classes of seafloor geodetic measurements [*Bürgmann and Chadwell*, 2014]. First, hybrid GPS-Acoustic (GPS-A) arrays measure the relative position between three or more seafloor transponders via acoustic ranging. The location of these transponders is monitored by a ship, buoy, or wave glider whose position is in turn monitored in a global reference frame using GPS. Second, pressure sensors can be deployed to the seafloor to directly measure vertical deformation. Finally, the seafloor can be imaged using a multibeam sonar array or an active source seismic array. These data have geodetic applications when comparing repeated surveys.

GPS-A was first proposed by *Spiess* [1985] and has since been employed to measure tectonic motions of the Juan de Fuca plate [*Chadwell and Spiess*, 2008], interseismic strain accumulation due to subduction offshore coastal Peru [*Gagnon et al.*, 2005], as well as the coseismic [*Sato et al.*, 2011; *Kido et al.*, 2011] and postseismic [*Watanabe et al.*, 2014; *Tomita et al.*, 2015] displacement due to the 2011 M_w 9.0 Tohoku-Oki earthquake. Analogous to terrestrial GPS, these systems can capture centimeter-scale motions at specific points, but GPS-A is hampered by the considerable expense of deploying and monitoring transponders as well as the significant ship time required to make the measurement. In contrast, multibeam sonar data are significantly cheaper to acquire and provide a denser spatial coverage like InSAR but are significantly less accurate. Repeated multibeam surveys have mostly been used to detect large changes (>10 m) in bathymetry due to volcanic events [*Chadwick et al.*, 1991; *Fox et al.*, 1992; *Chadwick et al.*, 1998; *Caress et al.*, 2012]. However, the *Fujiwara et al.* [2011] study showed that even the 10 m accuracy of the multibeam sonar was sufficient to provide

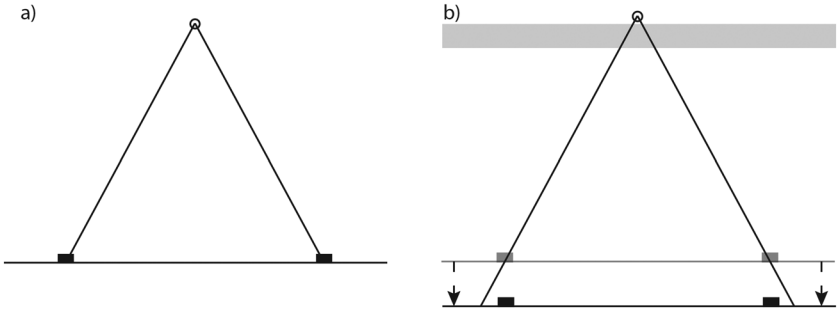

Figure 1. (a) Schematic cross section of a single multibeam ping ensonifying an area of seafloor and (b) its apparent change due to the injection of a horizontal layer of "slow" sound speed water near the sea surface.

important constraints on the very large displacement (~50 m) of the seafloor associated with the Tohoku-Oki earthquake. These multibeam data were critical for understanding why the tsunami had such large amplitude.

We are investigating methods for improving the accuracy of the seafloor displacement measurement using digital image correlation [*Pan et al.*, 2009], a technique used to measure horizontal offsets. Digital image correlation has been developed as a tool for measuring in-plane deformation with subpixel accuracy [*Chen et al.*, 1993; *Sjödahl and Benckert*, 1993]. These techniques are analogous to pixel tracking, which has been used in InSAR studies to measure ice velocities and along-track offsets for coseismic motions [*Joughin*, 2002].

The accuracy of a displacement measurement obtained from a correlation study is a subpixel quantity, but the horizontal resolution of standard multibeam bathymetry depends upon the height of the measurement platform above the seafloor. Thus, although *Fujiwara et al.* [2014] demonstrated meter accuracy displacement measurements from repeated multibeam surveys of shallow (~1000 m) water, this may not be easily extended to water deeper than 2000–3000 m, when the resolution of multibeam increases to 100–150 m. In contrast, sidescan data, while still having an along-track resolution comparable to bathymetry, have an across-track resolution R_r of

$$R_r = \frac{c\tau}{2\sin\theta} \tag{1}$$

where θ is the look angle, c is the speed of sound in seawater, and τ is the pulse length. (See Appendix 1) Since this quantity depends upon the look angle rather than platform height, the across-track resolution of sidescan may remain on the order of the pulse length in water 4000–6000 m deep. Here we evaluate sidescan data from a 12 kHz system having a nominal range resolution of 13–64 m. Thus, we propose cross-correlating the sidescan data product of multibeam sonar systems, which should yield superior displacement measurements in at least one dimension.

There are three general sources of error that must be quantified in such an experiment: variations in the sound speed profile, uncertainty in the digital image correlation that depend on the cruise parameters of the multibeam surveys (including the ship speed and stability, the seafloor depth and roughness, and the distance between repeat tracks), and limitations of the navigational system used to locate the measurement platform. We evaluate the error associated with each source by analyzing data from two cruises, the 2003 survey CNTL15RR collected approximately 2500 m above the young, lightly sedimented seafloor on the flank of the Juan de Fuca Ridge, and the 2010 survey MV1011 collected approximately 4300 m above old, heavily sedimented seafloor 300 nautical miles offshore Southern California.

1.2. Sound Speed Errors

We address concerns of sound speed variations with the following thought experiment. Consider the area of seafloor ensonified by right- and left-looking pings from a multibeam sonar (Figure 1a). We assume the most likely source of sound speed variations is due to internal waves in the upper water column. Such waves have a period on the order of tens of minutes, far greater than the duration of a single ping. Thus, we posit that at any given moment of time, the sound speed perturbation appears to be a horizontal layer, as shown in Figure 1b. This has the effect of introducing a time delay into the signal relative to the expected ping duration, similar to that if the platform had moved vertically some distance ΔH.

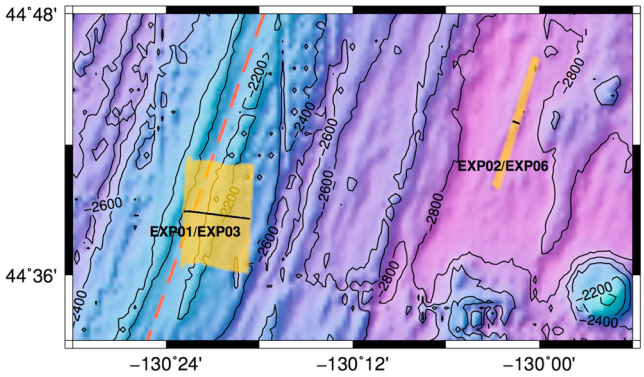

Figure 2. Regional bathymetry of the CNTL15RR cruise. The red dashed line marks the location of the Juan de Fuca Ridge. Locations of repeated tracks are displayed in black, with ensonified areas in yellow.

Due to the even symmetry of this model, we expect the apparent horizontal motion of the port and starboard seafloor to cancel one another. This expectation is routinely applied to address variations in sound speed velocity in high-precision GPS-Acoustic surveys [*Spiess et al.*, 1998]. The primary difference between GPS-Acoustic studies and repeat cross-correlation studies is that apparent horizontal motions due to sound speed velocity variations are averaged out over the time domain in the former and the spatial domain in the latter.

1.3. Image Correlation Errors

We assess the accuracy of the digital image correlation operation by applying it to sets of repeated sidescan sonar surveys, which have similar geometries in a single locale and consist of tracks collected in the same direction. We extract raw sidescan amplitudes from instrument-generated data files using the MB-System software package [*Caress and Chayes*, 1996] and rotate them into a coordinate frame with axes aligned with the along-track (azimuth) and across-track (range) directions. We then create grid files of the surveys using the Generic Mapping Tools software [*Smith and Wessel*, 1990]. We then calculate the normalized cross correlation between the grids, estimating the offset as the location of peak correlation coefficient [*Pan et al.*, 2009].

We analyze repeated multibeam tracks from the CNTL15RR and MV1011 cruises. These tracks are separated only by at most a few days of time; any deformation that may have occurred is thus negligible. We estimate the displacement accuracy by injecting an artificial horizontal offset in the repeat data and comparing the estimated offset with the injected offset. We repeat this process many times, analyzing the residuals between the injected and measured offsets to assess the accuracy and precision of this methodology.

In this way, we may begin to assess the relevance of various cruise parameters to this type of experiment. Of particular interest is the ship speed and stability during data collection, as well as how closely the tracks are repeated. These parameters should directly affect the distribution of soundings on the seafloor, as well as the coherence between repeat surveys. Also of interest are the seafloor characteristics; rougher seafloor should presumably lead to a higher correlation.

1.4. Navigation Errors

The multibeam sonar precisely measures the range of seafloor reflectors; such a relative measurement is only as accurate as our knowledge of the location of the instrument platform. Multibeam sonars generally rely on information from the ship navigation and motion reference unit to locate points on the seafloor. We evaluate the precision of the ship navigation by comparing it to independent location measurements collected during the CNTL15RR cruise, and apply the improved navigation to the associated sidescan data to assess its effect on the image correlation experiment.

2. Image Correlation Tests

2.1. CNTL15RR Cruise

A 2 day survey designed to assess the feasibility of creating synthetic aperture sonar images from multibeam sonar data collected in regions with deep (~3000 m) seafloor (Figure 2) was conducted in 2003 as part of the CNTL15RR cruise aboard the R/V *Roger Revelle*. The survey consisted of six tracks, denoted EXP01 through

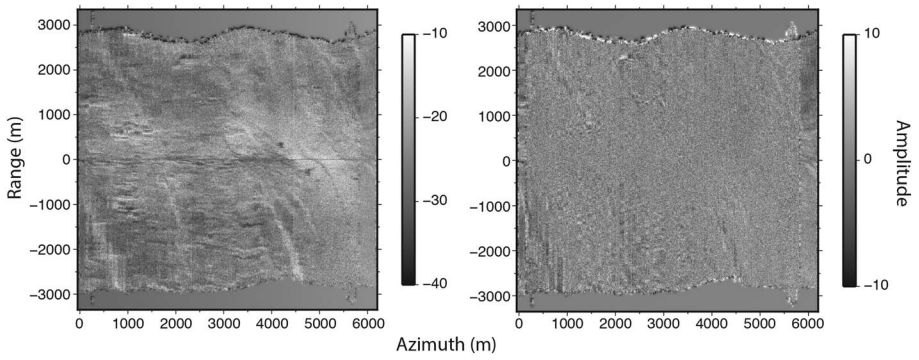

Figure 3. (left) Sum and (right) difference of the EXP01 and EXP03 sidescan tracks. The data have been rotated into a coordinate frame of range and azimuth, both in meters.

EXP06, in two sites, across the Juan de Fuca Ridge axis and off the ridge flank. Data were collected at slow ship speeds using a Kongsberg EM120 multibeam system.

Of the six multibeam tracks collected, EXP01 and EXP03 were collected above the Juan de Fuca Ridge axis with the intent of forming a synthetic aperture above young, rough seafloor. These data were collected at a speed of 0.5–1.5 knots (1 knot = 0.5 m/s = 1.85 km/h) and a heading of 277° and are a close repeat with a baseline of 1 m on average for 6 km of track length. We calculate an estimate of the signal and noise between these tracks by computing their sum and difference. The sum (Figure 3) shows a coherent mottled texture, and the difference shows a speckled pattern with little structure and relative amplitude about 25–50% of the coherent signal. The experiments had minor difficulties maintaining a constant heading due to persistent winds and currents from the north, but most correlation errors are likely due to the EM120 yaw stabilization being set to filtered heading during EXP01. As a result, the orientation of the pings in EXP01 was dependent upon the orientation of the ship at the time of transmission rather than upon a user-specified orientation. The yaw compensation of EXP03 was set to 273° to most closely match the heading of EXP01 while accounting for systematic biases between the ship's gyro system and the PHINS INU.

The EXP02 and EXP04 through EXP06 tracks were collected on the cleft flank of the Juan de Fuca Ridge near (44°42.75′N, −130°02.59′E). These surveys were designed to compliment the ridge axis surveys by forming a synthetic aperture above relatively old, more sedimented seafloor. The EXP02 track was collected at a speed of 0.5–0.6 knots and a heading of 290° controlled by the manual yaw stabilization. The remaining tracks were collected with the intent of repeating the EXP02 track, but were met by various difficulties. Inclement weather during EXP04 and EXP05 rendered the ship unable to maintain a steady track at such a slow ship speed; to compensate the ship speed was increased to 1.2–1.5 knots. To ensure that the pulse frequency of the sonar remained below the pulse repetition frequency theoretically required for successfully forming a synthetic aperture, the beam width was narrowed such that the maximum allowed range was 3800 m. As a result, EXP04 and EXP05 have drastically reduced coverage, and the coverage preserved is exclusively of the near-vertical beams unsuitable for digital image correlation due to their poor range resolution. The EXP06

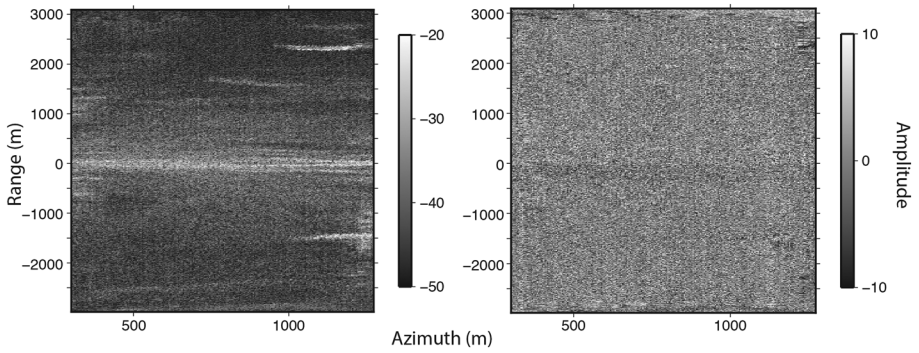

Figure 4. (left) Sum and (right) difference of the EXP02 and EXP06 sidescan tracks. The data have been rotated into a coordinate frame of range and azimuth, both in meters.

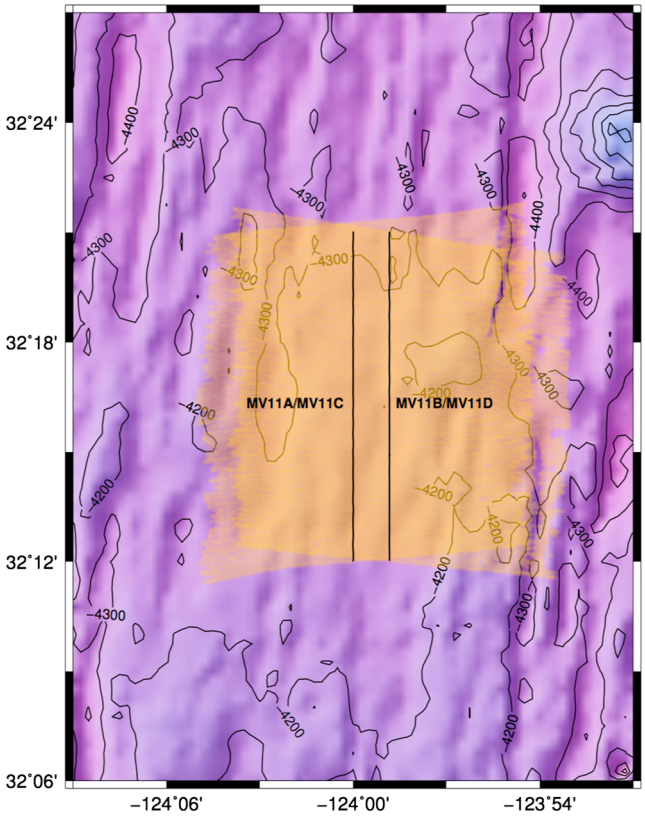

Figure 5. Regional bathymetry of the MV1011 cruise. Locations of repeated tracks are displayed in black, with ensonified regions in yellow.

track is a high-quality repeat of EXP02 since it was collected with the same heading and ship speed with a small baseline offset averaging 3 m but is only 1 km long due to time constraints during the survey. The horizontal lineations across the sidescan data (Figure 4) are sharp in the range direction, which aids in the cross correlation. In addition, the noise between surveys is small relative to the noise between EXP01 and EXP03.

2.2. MV1011 Cruise

The MV1011 cruise was conducted in 2010 offshore of Southern California in the vicinity of 124°W, 32.25°N using the Kongsberg EM122 multibeam array aboard the R/V *Melville* (Figure 5). The seafloor in this region is approximately 4300 m deep, being old and far from any spreading ridges. Presumably from its age, it is also heavily sedimented, although it displays a well-defined abyssal hill fabric oriented north-south. This is advantageous since the fabric manifests perpendicular to the range direction in the sidescan plots (Figures 6 and 7). The survey was collected at speed of 3.2 – 3.5 knots and includes five sections of track that repeat in two

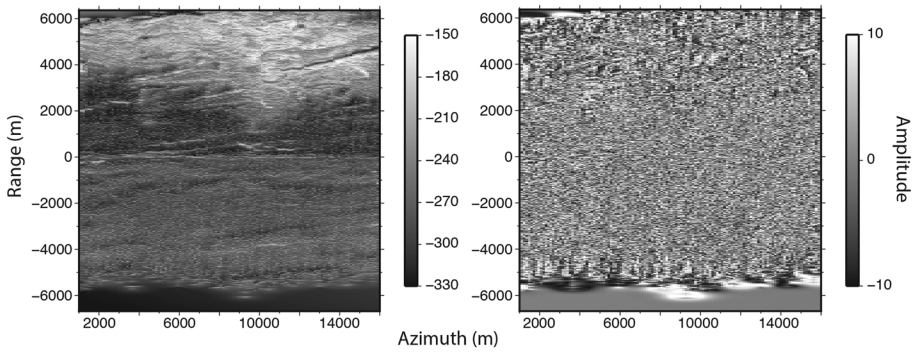

Figure 6. (left) Sum and (right) difference of the MV11A and MV11C sidescan tracks. The data have been rotated into a coordinate frame of range and azimuth, both in meters.

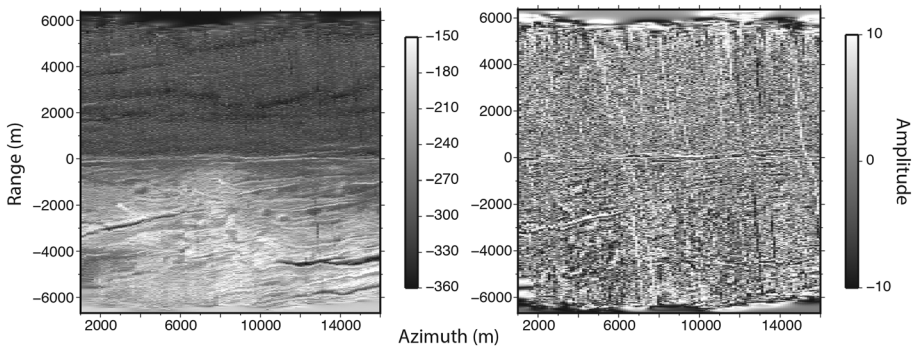

Figure 7. (left) Sum and (right) difference of the MV11B and MV11D sidescan tracks. The data have been rotated into a coordinate frame of range and azimuth, both in meters.

regions offset by approximately 2 km. The tracks that repeat one another are approximately 20 km long and separated by 2 m on average in the across-track direction. Denoting the successive repeated tracks MV11A through MV11E, MV11B, and MV11D repeat in the eastern section and the remainder in the western region. All of the tracks maintain a stable heading, although this heading is not necessarily in the direction of the track. Nevertheless, the stability of the heading means that we may easily correct for any resulting yaw biases. These tracks have a range sampling on the order of a meter, but an azimuth sampling between 30 and 40 m due to the faster ship speed compared to the CNTL15RR survey.

Although the ensonified areas of the western and eastern tracks show significant overlap, we do not perform correlation between the two sets for two reasons. First, the track headings are out of phase by approximately 180°, which may introduce unwanted errors due to the relative difference in the phase center of the multibeam array. Second, the 2 km offset between regions would likely reduce correlation significantly due to reflectors on the seafloor being observed by significantly different look angles. The error contributions of both of these effects will need to be quantified in the future, but the MV1011 survey is not ideal for such a study since the contributions cannot be isolated.

2.3. Results

We perform cross correlation of repeated raw sidescan tracks in the CNTL15RR and MV1011 surveys, injecting offsets in both the azimuth and range directions ranging from $-10 < x < 10$ m with 1 m increments. After estimating the displacement, we difference the measured and injected offsets to obtain a set of residuals with which to assess the efficacy of this method (Figure 8 and Table 1). For the cross correlation, the CNTL15RR tracks were gridded at a resolution of 20 m in both the azimuth and range directions. The MV1011 tracks were gridded at 120 m in the azimuth direction, owing to the scarcer ping spacing, and 20 m in the range direction.

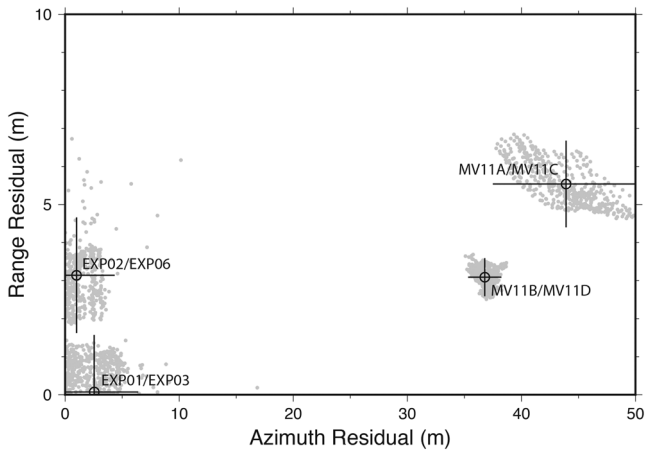

Figure 8. Absolute values of residuals obtained from correlation experiments comparing injected and measured displacements. Mean error and 2σ values are plotted for each experiment.

Table 1. Statistics of the Residuals Obtained by Differencing the Measured and Predicted Offsets Obtained by Performing Cross Correlation on the Whole Data Sets[a]

Experiments	Max Correlation	Azimuth Residual Mean (m)	Range Residual Mean (m)
EXP01/EXP03	0.58	2.55 ± 1.93	0.07 ± 0.75
EXP02/EXP06	0.80	1.01 ± 1.67	-3.14 ± 0.76
MV1011A/MV1011C	0.90	43.92 ± 3.21	-5.54 ± 0.57
MV1011B/MV1011D	0.90	-36.79 ± 0.73	3.09 ± 0.25

[a]CNTL15RR tracks EXP01-EXP06 were gridded at 20 m in both the azimuth and range directions. MV1011 tracks MV1011A-MV1011D were gridded at 120 m in the azimuth direction and 20 m in the range direction.

The residuals are precise to the scale of decimeters to meters, but show systematic biases on the order of meters to tens of meters.

3. Navigation Tests

3.1. Navigation Data

The location of the vessel is measured using the shipboard navigation, which depends upon a single-frequency GPS receiver processed using the P-code protocol (PC). During the CNTL15RR cruise, three additional dual-frequency GPS receivers were deployed aboard the vessel to serve as a complimentary location feed. From these dual-frequency GPS locations, we infer the orientation of the ship independent of the onboard motion reference unit and define a body frame through which we may accurately track the location of any specific point during the experiment. In particular, we are interested in the location of the center of gravity of the vessel (CG) and the location of the transmitter array (TX). For the following analysis, we shall be analyzing the location of the vessel during a 2 h window of the EXP03 repeat survey.

3.2. Location Differences

The locations of TX (based on dual-frequency GPS) and PC (based on single-frequency GPS) during the EXP03 survey are plotted in Figure 9. We take the difference between these time series and CG to analyze changes in relative position within the body frame of the ship. TX and PC have standard deviations of approximately 15 cm and 2 m, respectively (Table 2). However, the single-frequency ship navigation appears to drift with respect to the body frame defined by the dual-frequency receivers on the order of 1 m/h, as demonstrated by the apparent shift in the location of PC (Figure 10). The actual precision of PC is overestimated by the standard deviation due to this drift and is likely closer to ~50 cm.

We repeat the digital image correlation procedure for EXP01 and EXP03 using the locations of CG as measured by the dual-frequency GPS units (Table 3). The residuals of the reprocessed results show a smaller mean and larger standard deviation in both the azimuth and range direction.

4. Discussion

We derive our estimate of the accuracy and precision of the displacement measurement between two surveys as the mean and standard deviation of the residuals (Table 1 and Figure 8). The first-order estimate of

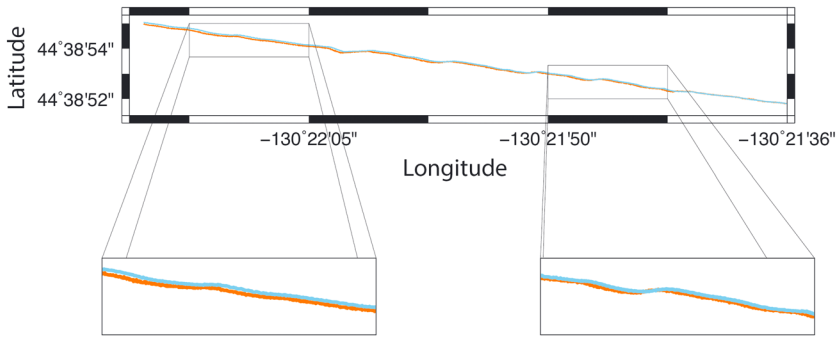

Figure 9. EXP03 track as recorded by TX (blue) and PC (orange). Boxed sections are zoomed in to demonstrate instrument drift.

Table 2. Position Differences and Absolute Distances Between Reference Points as Measured by Dual-Frequency GPS Units

Points	E-W Position (m)	N-S Position (m)
TX - CG	14.133 ± 0.067	-0.692 ± 0.132
PC - CG	14.783 ± 1.719	-1.341 ± 0.945

the accuracy of this method comes from the mean of the residuals, since any biases in the data will cause the mean to deviate from zero. We observe biases on the order of meters that increase by an order of magnitude in the along-track (azimuth) dimension at faster ship speeds. The large (>30 m) azimuthal biases of the MV1011 residuals may result from the lower ping density arising from these faster surveys. There is likely a shift in the ping locations along track between the two surveys, resulting in the surveys ensonifying slightly different portions of the seafloor within the same area. Increases in range bias due to ship speed are not directly observed, since the echo density depends upon the sampling rate in the range direction rather than the ship speed. However, we predict that faster ship speed could cause decorrelation between tracks if the ping shift is greater than half the wavelength of the measured features; this would adversely affect both the azimuth and range accuracy.

Observed biases may be partially due to variations in the sound speed profile between surveys. Such variations have been previously observed [*Spiess et al.*, 1998], but on the order of decimeters. In addition, we expect the apparent displacements from sound speed variations to mostly cancel due to symmetry. These errors are likely due to shortcomings of the ship navigation since updating the navigation with locations constrained using a trio of dual-frequency GPS receivers significantly reduced the biases observed in the EXP01/EXP03 tracks (Table 3). This is consistent with a drift we observed in the single-frequency ship navigation, which is on the order of meters per hour. This drift is likely due to changing electron content in the ionosphere and probably contributes to a significant portion of the error observed in the correlation experiment. Although errors introduced by these effects may not be crippling for most marine applications, they are large enough that a single-frequency GPS is insufficient for geodetic applications at sea.

The precision of these measurements may be estimated from the standard deviation of the residuals, and lies within the range of 0.5–2 m in the range dimension and 1–10 m for the azimuthal direction (Figure 8 and Table 1). This difference in precision is expected due to the inherently higher resolution of sidescan sonar in the range direction, especially at faster ship speeds. We interpret the improved range precision of the MV1011 tracks as due to the lineations parallel to the range dimension, which provide a distinct signal in the correlation. Geodetic measurements at this precision should be sufficient to measure displacement due to offshore earthquakes, but only once the biases due to ship speed and navigation constraints have been minimized. Even with minimal bias, signals such as plate motions would require long periods of time between measure-

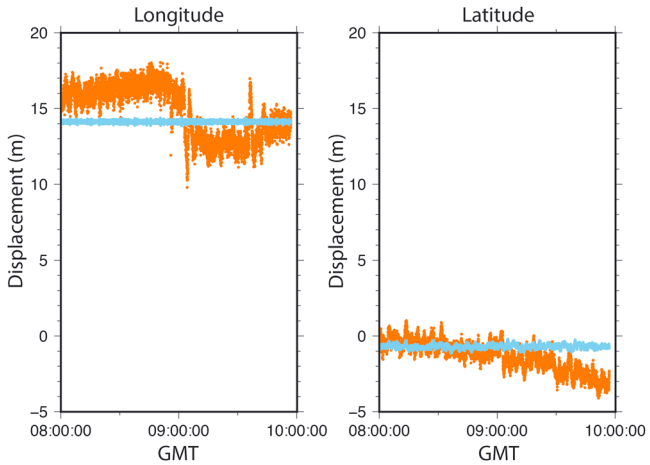

Figure 10. Locations of TX (blue) and PC (orange) relative to CG. Longitude and latitude differences are converted to meters for ease of comparison with other error sources.

Table 3. Statistics of the Residuals Obtained by Digital Image Correlation for EXP01/EXP03, Varying Navigation Data Used for Processing[a]

Navigation	Max Correlation	Azimuth Residual Mean (m)	Range Residual Mean (m)
PC	0.58	2.55 ± 1.93	0.07 ± 0.75
CG	0.55	0.48 ± 4.52	0.01 ± 1.66

[a]Tracks were gridded at 20 m.

ments. Since measurements are more accurate in the range dimension, we recommend conducting at least two orthogonal surveys in an area of interest, one for each horizontal dimension.

The seafloor roughness does not seem to play a large role in the displacement precision since tracks over smooth seafloor such as EXP02/EXP06 produce displacement measurements roughly as precise as tracks over rougher seafloor. This phenomenon has been previously observed by *Schreier et al.* [2000], who posited that the long-wavelength features contribute the largest component of the correlation. We verify this explicitly by computing the coherency spectrum for each pair of repeated tracks in the across-track (range) dimension (Figure 11). In each case the coherency is highest at low wave number (long wavelength) and falls to a noise floor at higher wave numbers (short wavelengths). We attribute more gradual decline of the MV1011 spectra to a more even frequency distribution arising from the lineations parallel to the range dimension. The approximate wavelength at which three of the four coherency spectra fall below 0.2 is 100 m or 5 pixels, since all of the grids considered in this study have a range cell size of 20 m. This may seem unintuitive since the high contrast from the high-frequency signal of a rough seafloor should presumably create a higher correlation, but in practice these features are also more susceptible to random noise.

These measurements are limited by the quality of the seafloor model used to define the range parameter. For these studies a flat seafloor model has been sufficient, but in areas with sufficient relief it may be necessary to define a more rigorous range coordinate. In addition, these measurements must still be converted to a geographic coordinate frame; they are thus limited by the quality of the digital elevation model used in the conversion. Note, however, that multibeam is somewhat unique in that the bathymetry data product may serve this role. There is also some ambiguity in how the measurements from this study would map into the geographic coordinate frame since they are derived from data on both the port and starboard of the vessel. However, this ambiguity could be resolved by correlating smaller data subsets, which would also allow us to more easily discard lower quality data such as those near-vertical incidence. We have yet to implement a code to perform either of these operations.

Unfortunately, the cross correlation is dependent upon the gridding parameters used to process the data. The grid cell size should be large enough to include multiple samples, which are then averaged to reduce noise.

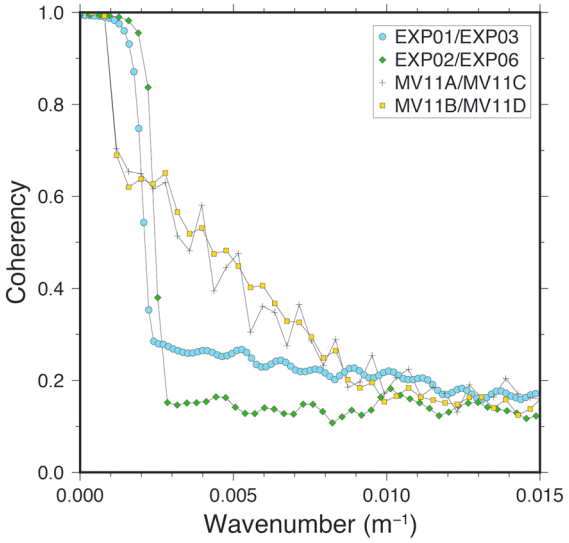

Figure 11. Coherency spectra in the across-track (range) dimension, computed for each pair of repeated tracks.

However, cells that are too large are less sensitive to the displacements we wish to measure. The cell size in the range dimension is primarily governed by the sampling rate of the instrument, while the azimuthal cell size is governed by the ping spacing, a function of the ship speed. While we expect the slower surveys to have better accuracy in the azimuthal direction due to denser pings, we do not observe this effect. This is likely due to the unstable heading of the ship at such slow speeds, which causes the pings to have variable density. It is thus just as important that a multibeam survey have a steady orientation as a slow speed for geodetic application.

5. Conclusions

We measure simulated seafloor displacement using repeated sidescan sonar surveys. From a platform height of 3–4 km and a ship speed of 0.5–3.5 knots, we are able to measure displacements accurate to tens of meters in the along-track (azimuth) direction and meters in the across-track (range) direction, an improvement over the previous *Fujiwara et al.* [2011] study of approximately 1 order of magnitude. These measurements are limited by the accuracy of the shipboard navigational system, which may be accurate to ~10 cm if it utilizes a dual-frequency GPS. Single-frequency GPS units drift on the order of meters per hour and are thus not sufficiently accurate to be applied for geodetic purposes.

The greater accuracy and precision of these measurements in the range dimension has direct implications for the orientation of the optimal survey layout. It is most advantageous to have the expected deformation occur in the across-track direction or some component thereof. Taking the example of surveying a subduction zone, we recommend collecting at least two tracks of data, which are oriented either parallel or at angles to the trench, rather than one track across the trench.

For this experimental setup to work, the survey must be collected at a stable heading and relatively slow speed. In addition, it is important to keep a careful record of the original survey so that it may be closely repeated at a later time. However, since this experimental setup makes exclusive use of equipment already available on most research vessels (except dual-frequency GPS), it presents an economical alternative to more traditional seafloor geodetic methods and may be implemented in conjunction with a wide variety of other seagoing research.

Appendix A: Methods

A1. Overview

We solve for the displacement between two multibeam surveys by computing the correlation between them. This method has been previously applied to measure vertical bathymetry changes due to submarine volcanic eruptions [*Fox et al.*, 1992; *Chadwick et al.*, 1991, 1998; *Caress et al.*, 2012]. In addition, analogous correlation techniques have been used to measure horizontal displacements [*Fox et al.*, 1992; *Fujiwara et al.*, 2011]. However, all of these previous studies have only considered the bathymetry product from the multibeam sonar; our innovation is applying these techniques to the sidescan data produced alongside the bathymetry.

A2. Sidescan Versus Multibeam Resolution

What makes sidescan attractive for use in these types of correlation studies is its resolution. The azimuth and range resolution (roughly corresponding to the along-track and across-track resolution) of multibeam bathymetry are governed by Fraunhoffer diffusion, which simplifies to

$$R_f = \frac{\rho\lambda}{L} \tag{A1}$$

where R_f is the resolution, ρ is the slant range, λ is the pulse wavelength, and L is the aperture length. This is suboptimal because the parameter ρ is dependent upon the depth of the seafloor.

In the case of sidescan, only the azimuth resolution is governed by Fraunhoffer diffusion; the range resolution is

$$R_r = \frac{c\tau}{2\sin\theta} \tag{A2}$$

where θ is the look angle, c is the speed of sound in seawater, and τ is the pulse length.

For reference, a Kongsberg EM120 multibeam sonar, which has a pulse length of 15 ms and an aperture length of 7 m, may have a bathymetry resolution of 100–150 m in both the along-track and across-track directions for seafloor of approximately 3000 m depth. The range resolution of the corresponding sidescan would be an undefined quantity at vertical incidence, but improve to about 65 m for a look angle of 10°and 13 m at 60°. As a result, sidescan data offers superior resolution in at least one dimension.

A3. Constructing Coordinate Axes

The EM120 has nine cross-track sectors that are constrained by both the direction and carrier frequency of the outgoing pulse. The raw sidescan amplitudes do not have specific range values given by the instrument. Rather, there is information about the sector each pixel falls into and the range of each sector's center pixel. We wish to construct a simple range model, but the given center pixel associated with the minimum range may not correspond to the actual pixel with minimum range because there can be many pixels with irregular spacing in a given sector. We solve for the center pixel explicitly by fitting a linear trend to the sets of center pixel ranges of the port and starboard beams. The center pixel corresponds to the minimum where these two trends intersect. From the location of the center pixel, we may define a coordinate frame of relative ranges by incrementing the range of any adjacent pixels by a factor of $c/2\nu$, where c is assumed 1500 m/s, and ν is the sampling rate. Although this exercise does not yield absolute ranges, we may use it to easily construct ranges for a given seafloor model, which for the purposes of this paper will correspond to a flat seafloor of depth H.

We define the along-track, or azimuth, coordinate using locations recorded by the ship navigation system every ping. To create a consistent coordinate axis, we define an ideal repeat track line by performing a least squares fit on the locations recorded in both surveys. The critical information is then contained within the displacement vector between the ship's location and an arbitrary reference point along the ideal repeat track. Decomposing this displacement vector into components parallel and perpendicular to the ideal repeat track yields the azimuth coordinate we desire and a location bias, which we refer to as the sway. Of course, the magnitude of the azimuth depends strongly on the location of the reference point; we prefer to choose a point sufficiently far from the ship surveys such that the sway is much smaller in magnitude than the azimuth in an effort to minimize distortions in the coordinate.

A4. Coordinate Axis Corrections

Once we have defined the range and azimuth coordinates, we must align the tracks by correcting their coordinates based upon deviations in the ship position and orientation from the heading and location presumed by the ideal repeat track. In the following section, we shall define two such corrections based upon the sway (horizontal across-track motion) and yaw (heading). Presumably, there are analogous corrections for the surge, heave, roll, and pitch, but we shall not be taking these into account for the following reasons. The surge correction is somewhat trivial in that it is parallel to the azimuth coordinate. Corrections to the heave are analogous to variations in tidal height as well as sound speed in the upper water column. The roll (side-side rocking of the vessel), while critical for forming the multibeam bathymetry, is unnecessary for sidescan for similar reasons as the surge; our definition of the look angle is arbitrarily dependent upon whatever model we use the describe the seafloor. The pitch (fore-aft rocking) can vary on timescales shorter than the length of a ping and is thus an ill-posed correction.

The sway correction accounts for strictly lateral deviations of the ship location from the ideal repeat track for a given azimuth. These deviations are easily measurable while creating the azimuth coordinate frame, and will always be present since perfectly repeating ship tracks are nominally very difficult, if not impossible, to obtain.

The need for the correction then arises since the range is taken at face value to be from the ideal ship track, but in this case would mislocate the reflectors by the ship sway Δr. The magnitude of the correction $\Delta\rho_h$ may be calculated by making a parallel ray approximation, allowing us to write the relationship

$$\Delta\rho_h = \Delta r \sin\theta \tag{A3}$$

$$\cos\theta = \frac{H}{\rho} \tag{A4}$$

By this relationship, we see that the sway increases the range from the ideal repeat track line to reflectors on the same side as the offset, and decrease the range to reflectors on the opposite side. This may easily be verified qualitatively by inspection of Figure A1.

We must also account for variations in the ship heading. Nominally, the range coordinate is orthogonal to the azimuth coordinate, which in turn is parallel to the ideal repeat ship track. However, the range is actually perpendicular to the instantaneous heading of the ship; deviations of this from the ideal track will rotate the range axis, causing the reflectors sensed by the array to be mislocated in both azimuth and range.

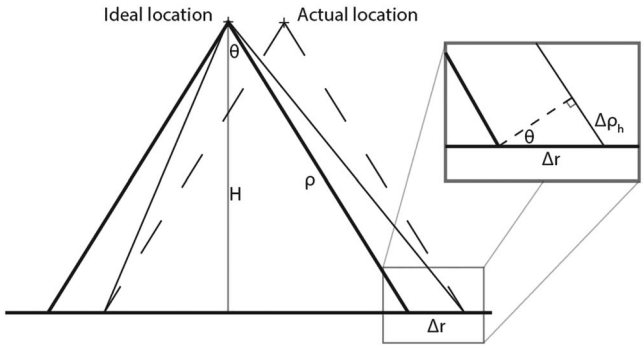

Figure A1. Schematic diagram of the range correction required to account ship sway. The ideal uncorrected range measurement is shown by the thick lines, which are offset from the actual measurements shown by the dashed line by some distance Δr. For the correlation between the repeated tracks, we require the corrected ranges from the ideal ship location along the repeated track and the actual reflectors, shown by the thin solid lines. The ship track is into the page.

For a given reflector measured by a ship with yaw deviation α, we may form a right triangle with the measured range to the reflector as the hypotenuse and the azimuth correction and corrected range as the legs (Figure A2). We may then write the range correction as

$$\cos\alpha = \frac{(\rho + \Delta\rho_\alpha)\sin\theta}{\rho\sin\theta} \tag{A5}$$

$$\Delta\rho_\alpha = \rho(\cos\alpha - 1) \tag{A6}$$

Note that the range correction is by definition always negative. In addition, we are implicitly assuming that the look angle of the corrected range is approximately equivalent to the look angle of the actual range. This should be reasonable as long as α is sufficiently small. The corresponding azimuth correction is

$$\Delta a_\alpha = \rho\sin\alpha\sin\theta \tag{A7}$$

The azimuth correction will be positive on one side of the ship and negative on the other side.

The errors due to horizontal baseline shifts display an odd symmetry that causes them to map directly as an apparent horizontal shift of the seafloor. Luckily, this baseline is easy to measure as it can be directly solved for alongside the azimuth coordinate. Another reason why the horizontal baseline contributes a larger error is due simply to the difficulty of exactly repeating ship tracks. This correction is bounded by Δr, which could easily be many tens or even hundreds of meters.

The corrections due to the orientation of the vessel are remarkably similar, showing similar magnitudes for the azimuth and range corrections. The range correction due to the orientations show an even symmetry and may have a magnitude of a few meters to a few tens of meters, assuming a range on the order of 5000 m. The azimuth correction is much larger in magnitude, being on the order of a few tens to hundreds of meters and rotating the coordinate frame.

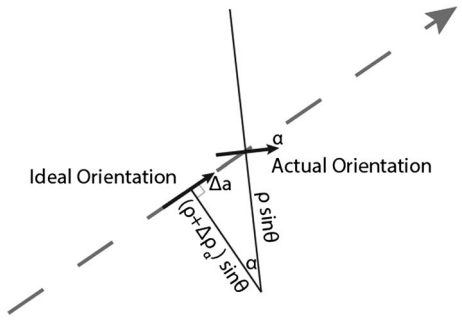

Figure A2. Schematic diagrams of the range correction required due to errors in the ship heading. The perspective is a bird's eye view upon the ideal repeat ship track.

However, it may not always be necessary to apply the correction for the ship's heading, as the sonar has a yaw stabilization system that, when operating, automatically aligns the ping with the average course of the ship, eliminating the need for this correction. In addition, it may be unreasonable to apply a correction due to the pitch, which varies on the order of seconds and goes through multiple cycles over the course of a single ping.

A5. Data Correlation

Before performing cross correlation on the two data sets, we must first transcribe them into coregistered grid files. We do so using algorithms from the Generic Mapping Tools (GMT) programming suite [*Smith and Wessel*, 1990]. We first mitigate the effects of any outliers by performing a blockmedian, which returns the median amplitude of the pixels that fall within grid cells defined by the user. We may then create the grid using the algorithm xyz2grd. During this process, the grids are coregistered as long as they have the same bounds and cell size; both are easy for the user to manipulate.

Alternatively, grids may be generated using the GMT algorithm surface, which uses a tension spline to fit the data. Using this method, we recommend a tension factor of 0.4 for gridding sidescan data, as opposed to the tension of 0.35 recommended by *Smith and Wessel* [1990] and used by *Fujiwara et al.* [2011]. We have also found our best results by using a convergence limit of 0.08 to prevent the spline from introducing high-frequency noise into the grid.

We calculate the normalized cross-correlation criteria, as it has been shown to be the most stable correlation criterion [*Pan et al.*, 2006]. We compute the cross correlation for pixel offsets within a user-defined search radius of some initial guess of deformation [*Pan et al.*, 2009]. We define the displacement between the two surveys as being the displacement that yields the maximum correlation [*Sjödahl and Benckert*, 1993]; by fitting an appropriate function to the correlation peak we may obtain the displacement to subpixel accuracy. We have found an appropriate model to be that of a Gaussian peak, as long as we only consider points in the neighborhood of the maximum. Coincidentally, only having to compute the correlation in the neighborhood of the peak drastically reduces the required computation time. This method is easily able to discern subpixel offsets, but is subject to a few limitations, the most obvious being that the user must have an appropriate guess before running the algorithm. A more subtle limitation is that this algorithm is most sensitive to displacements near the initial guess. As the guess may be iteratively improved, this algorithm is least accurate for offsets exactly halfway between pixels.

Acknowledgments

This work was supported by the National Science Foundation, Marine Geology and Geophysics division, grant OCE-1536386. Data are available through the National Centers for Environmental Information (NCEI) bathymetric data viewer, accessible at https://maps.ngdc.noaa.gov/viewers/bathymetry/.

References

Bürgmann, R., and D. Chadwell (2014), Seafloor geodesy, *Ann. Rev. Earth Planet. Sci.*, *42*(1), 509–534.

Bürgmann, R., P. A. Rosen, and E. J. Fielding (2000), Synthetic aperture radar interferometry to measure Earth's surface topography and its deformation, *Ann. Rev. Earth Planet. Sci.*, *28*(1), 169–209, doi:10.1146/annurev.earth.28.1.169.

Caress, D. W., and D. N. Chayes (1996), Improved processing of hydrosweep DS multibeam data on the R/V Maurice Ewing, *Mar. Geophys. Res.*, *18*(6), 631–650.

Caress, D. W., D. A. Clague, J. B. Paduan, J. F. Martin, and B. M. Dreyer (2012), Repeat bathymetric surveys at 1-metre resolution of lava flows erupted at axial seamount in April 2011, *Nat. Geosci.*, *5*, 483–488.

Chadwell, C. D., and F. N. Spiess (2008), Plate motion at the ridge-transform boundary of the south cleft segment of the Juan de Fuca Ridge from GPS-acoustic data, *J. Geophys. Res.*, *113*, B04415, doi:10.1029/2007JB004936.

Chadwick, W. W., R. W. Embley, and C. G. Fox (1991), Evidence for volcanic eruption on the Southern Juan de Fuca Ridge between 1981 and 1987, *Nature*, *350*(6317), 416–418.

Chadwick, W. W., R. W. Embley, and T. M. Shank (1998), The 1996 Gorda Ridge eruption: Geologic mapping, sidescan sonar, and seabeam comparison results, *Deep Sea Res., Part II*, *45*(12), 2547–2569, doi:10.1016/S0967-0645(98)000836.

Chen, D. J., F. P. Chiang, Y. S. Tan, and H. S. Don (1993), Digital speckle-displacement measurement using a complex spectrum method, *Appl. Opt.*, *32*(11), 1839–1849, doi:10.1364/AO.32.001839.

Davis, J. L., Y. Fialko, W. E. Holt, M. M. Miller, S. E. Owen, and M. E. Pritchard (Eds.) (2012), A foundation for innovation: Grand challenges in geodesy, Rep. from the Long-Range Science Goals for Geodesy Community Workshop, 79 pp., UNAVCO, Boulder, Colo.

Fox, C. G., W. W. Chadwick, and R. W. Embley (1992), Detection of changes in ridge-crest morphology using repeated multibeam sonar surveys, *J. Geophys. Res.*, *97*(B7), 11,149–11,162, doi:10.1029/92JB00601.

Fujiwara, T., S. Kodaira, T. No, Y. Kaiho, N. Takahashi, and Y. Kaneda (2011), The 2011 Tohoku-oki earthquake: Displacement reaching the trench axis, *Science*, *334*, 1240.

Fujiwara, T., Y. Masaki, and F. Yamamoto (2014), Evaluation of spatial resolution and estimation error of seafloor displacement observation from vessel-based bathymetric survey by use of AUV-based bathymetric data, *Mar. Geophys. Res.*, *36*(1), 45–60, doi:10.1007/s11001-014-9242-8.

Gagnon, K., C. D. Chadwell, and E. Norabuena (2005), Measuring the onset of locking in the Peru-Chile trench with GPS and acoustic measurements, *Nature*, *434*(7030), 205–208.

Joughin, I. (2002), Ice-sheet velocity mapping: A combined interferometric and speckle-tracking approach, *Ann. Glaciol.*, *34*(1), 195–201, doi:10.3189/172756402781817978.

Kido, M., Y. Osada, H. Fujimoto, R. Hino, and Y. Ito (2011), Trench-normal variation in observed seafloor displacements associated with the 2011 Tohoku-Oki earthquake, *Geophys. Res. Lett.*, *38*, L24303, doi:10.1029/2011GL050057.

Pan, B., H. Xie, B. Xu, and F. Dai (2006), Performance of sub-pixel registration algorithms in digital image correlation, *Meas. Sci. Technol.*, *17*(6), 1615.

Pan, B., K. Qian, H. Xie, and A. Asundi (2009), Two-dimensional digital image correlation for in-plane displacement and strain measurement: A review, *Meas. Sci. Technol.*, *20*(6), 62001.

Sato, M., T. Ishikawa, N. Ujihara, S. Yoshida, M. Fujita, M. Mochizuki, and A. Asada (2011), Displacement above the hypocenter of the 2011 Tohoku-Oki earthquake, *Science*, *332*(6036), 1395.

Schreier, H. W., J. R. Braasch, and M. A. Sutton (2000), Systematic errors in digital image correlation caused by intensity interpolation, *Optical Engineering*, *39*(11), 2915–2921, doi:10.1117/1.1314593.

Sjödahl, M., and L. R. Benckert (1993), Electronic speckle photography: Analysis of an algorithm giving the displacement with subpixel accuracy, *Appl. Opt.*, *32*(13), 2278–2284, doi:10.1364/AO.32.002278.

Smith, W., and P. Wessel (1990), Gridding with continuous curvature splines in tension, *Geophysics*, *55*(3), 293–305, doi:10.1190/1.1442837.

Spiess, F. N. (1985), Suboceanic geodetic measurements, *IEEE Trans. Geosci. Remote Sens.*, *GE-23*, 502–510.

Spiess, F. N., C. D. Chadwell, J. A. Hildebrand, L. E. Young, G. H. Purcell Jr., and H. Dragert (1998), Precise GPS/Acoustic positioning of seafloor reference points for tectonic studies, *Phys. Earth Planet. Inter.*, *108*, 101–112.

Tomita, F., M. Kido, Y. Osada, R. Hino, Y. Ohta, and T. Iinuma (2015), First measurement of the displacement rate of the Pacific Plate near the Japan Trench after the 2011 Tohoku-Oki earthquake using GPS/acoustic technique, *Geophys. Res. Lett.*, 8391–8397, doi:10.1002/2015GL065746.

Watanabe, S.-I., M. Sato, M. Fujita, T. Ishikawa, Y. Yokota, N. Ujihara, and A. Asada (2014), Evidence of viscoelastic deformation following the 2011 Tohoku-Oki earthquake revealed from seafloor geodetic observation, *Geophys. Res. Lett.*, *41*, 5789–5796, doi:10.1002/2014GL061134.

Wdowinski, S., Y. Sudman, and Y. Bock (2001), Geodetic detection of active faults in S. California, *Geophys. Res. Lett.*, *28*(12), 2321–2324, doi:10.1029/2000GL012637.

Wilcock, W., P. Bodin, J. Delaney, J. Vidale, and Conveners (2012), Workshop report on seafloor geodesy in Cascadia June 11–12, 2012, Univ. of Washington in Seattle, Washington.